University of Groningen

Type II Homo-Type Bi$_2$O$_2$Se Nanosheet/InSe Nanoflake Heterostructures for Self-Driven Broadband Visible-Near-Infrared Photodetectors

Zhang, Zhiyang; Han, Lixiang; Dan, Zhiying; Li, Hengyi; Yang, Mengmeng; Sun, Yiming; Zheng, Zhaoqiang; Huo, Nengjie; Luo, Dongxiang; Gao, Wei

IMPORTANT NOTE: You are advised to consult the publisher's version (publisher's PDF) if you wish to cite from it. Please check the document version below.

Document Version
Publisher's PDF, also known as Version of record

[Link to publication in University of Groningen/UMCG research database](#)

Type II Homo-Type Bi$_2$O$_2$Se Nanosheet/InSe Nanoflake Heterostructures for Self-Driven Broadband Visible−Near-Infrared Photodetectors

Zhiyang Zhang, Lixiang Han, Zhiying Dan, Hengyi Li, Mengmeng Yang, Yiming Sun, Zhaoqiang Zheng, Nengjie Huo, Dongxiang Luo, Wei Gao,* and Jingbo Li*

Read Online

ACCESS | Metrics & More | Article Recommendations | Supporting Information

ABSTRACT: Bi$_2$O$_2$Se nanosheets, an emerging ternary non-van der Waals two-dimensional (2D) material, have garnered considerable research attention in recent years owing to their robust air stability, narrow indirect bandgap, high mobility, and diverse intriguing properties. However, most of them show high dark current and relatively low light on/off ratio and slow response speed because of the large charge carrier concentration and bolometric effect, hindering their further application in low-energy-consuming optoelectronics. Herein, a homotype van der Waals heterostructure based on exfoliated n-InSe integrated with chemical vapor deposition (CVD)-grown n-Bi$_2$O$_2$Se nanosheets that have type II band alignment was fabricated. The efficient interfacial charge separation, strong interlayer coupling, and effective built-in electric field across the heterointerface demonstrated excellent, stable, and broadband self-driven photodetection in the range 400−1064 nm. Specifically, a high responsivity (R) of 75.2 mA·W^{-1} and a high specific detectivity (D^*) of 1.08×10^{12} jones were achieved under 405 nm illumination. Additionally, a high R of 13.3 mA·W^{-1} and a high D^* of 2.06×10^{11} jones were achieved under 980 nm illumination. Meanwhile, an ultrahigh I_{light}/I_{dark} ratio over 10^5 and a fast response time of 5.8/15 ms under 405 nm illumination confirmed the excellent photosensitivity and fast response behavior. Furthermore, R could be enhanced to 13.6 and 791 mA·W^{-1} under 405 and 980 nm illumination at a drain−source voltage (V_{ds}) of 1 V, respectively, originating from a lower potential barrier. This study suggested that the Bi$_2$O$_2$Se nanosheet/InSe nanoflake homotype heterojunction can offer potential applications in next-generation broadband photodetectors that consume low energy and exhibit high performance.

KEYWORDS: Bi$_2$O$_2$Se, InSe, van der Waals heterostructure, type II band alignment, photovoltaic effect
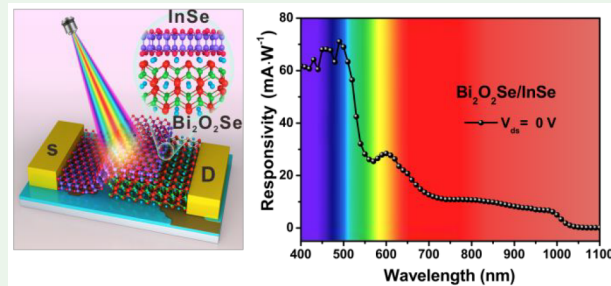
INTRODUCTION

Atomically thin two-dimensional (2D) materials including graphene, MoS$_2$, InSe, and black phosphorus (BP) with novel physical properties such as moiré physics, valley effects, and quantum Hall effect have shown promising applications in optoelectronics, sensors, memristors, logic circuits, photonic integrated circuits, meta-optics, and nanomechanical resonators over the past two decades.[1−6] Benefiting from the dangling-bond free interfaces of 2D materials and synergistic effect, van der Waals (vdWs) heterojunctions formed by weak vdWs forces offer considerable freedom to design multifunctional devices with substantially improved performances compared to individual components without the issue of lattice mismatching.[7−11] Among them, p−n or n−n or p−p vdWs heterojunctions with type II staggered band alignment can considerably promote the separation of carriers and offer numerous applications in the field of next-generation ultrafast photodetection, sensing, and solar energy harvesting.[12]

Recently, an n-type Bi$_2$O$_2$Se nanosheet, a novel ternary 2D material with a narrow bandgap in the range 0.11−1.27 eV, an interlayer spacing of 0.61 nm, and a small electron effective mass of 0.14m_0, has garnered tremendous attention. This is because it has an ultrahigh carrier mobility of over 20000 cm^2·V^{-1}·s^{-1} at 2 K and robust stability and other intriguing physical properties, such as ferroelectricity, strong spin−orbit coupling, piezoelectricity, bolometric effect, and high permittivity.[13−20] Furthermore, various approaches, such as mechanical exfoliation, the chemical vapor deposition (CVD) method, the solution-assisted method, and molecular beam epitaxy have been reported for preparing Bi$_2$O$_2$Se nanosheets on different
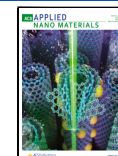
substrates.[21−24,26,27] Recently, the vdWs heterostructures based on Bi_2O_2Se nanosheets have demonstrated high photo-detection performance.[28−36] For instance, Yang et al. reported a 2D photodetector based on an n-$MoSe_2$/Bi_2O_2Se homotype heterostructure with a high responsivity (R) of 413.1 mA· W^{-1}.[37] However, the loss of a self-driven function, the relatively slow response time of 0.79/0.49 s, and the limited response spectrum from 405 to 808 nm of this photodetector need to be improved. Meanwhile, Zhai et al. reported a p-WSe_2/n-Bi_2O_2Se vdWs heterojunction photodiode, achieving an ultrahigh rectification ratio of 10^5 attributed to a large band offset.[38] However, this excellent photovoltaic performance is only focused on the visible wavelength without highlighting the broadband light absorption of bare Bi_2O_2Se nanosheets. Moreover, some insufficient phenomena such as self-driven loss, ultralow R, ordinary specific detectivity ($D*$), and a complicated transfer process have been seen in other Bi_2O_2Se nanosheet-based heterostructures such as n-WS_2/Bi_2O_2Se, Bi_2Te_2Se/Bi_2O_2Se, Bi_2Se_3/Bi_2O_2Se, and p-Te/Bi_2O_2Se.[39−43]

Most of the 2D materials in few-layered or multilayered structures integrated with Bi_2O_2Se always feature an indirect bandgap, suffering from relatively weak light−matter inter-action. Although BP is a direct bandgap 2D material that is independent of the number of layers and the vdWs heterojunctions based on Bi_2O_2Se/BP possess high photo-detection performance,[34,44] the intrinsic instability of BP hinders its wide application.[45,46] Additionally, monolayer 2D materials such as WS_2 and MoS_2 with direct bandgap show a relatively low light absorption coefficient and low responsivity. The multilayered β-InSe nanoflake (>6 nm) with the merits of tunable electronic properties, broadband photoresponse, and a high light absorption coefficient has a direct bandgap ~1.25 eV. Therefore, it can exhibit high light−matter interaction and a strong photon excitation energy for high-performance photodetectors.[47−50] According to the theoretical band structure, incorporating the multilayered InSe nanoflakes can directly improve the visible−near-infrared photodetection of the Bi_2O_2Se nanosheets for designing a homotype vdWs heterostructure with a theoretical type II band alignment.

Herein, a Bi_2O_2Se nanosheet/InSe nanoflake homotype heterostructure was reported by directly stacking the exfoliated multilayered InSe onto the CVD-grown Bi_2O_2Se nanosheet via a dry transfer method, as shown in Scheme 1. The efficient interlayer charge transfer, strong coupling effect, and type II band alignment were confirmed by using the Raman spectroscopy and photoluminescence (PL) measurements. This photodiode exhibits a moderate rectification ratio of 230 and an ideal factor of 1.19. Additionally, the photodiode had a fast response to the broadband spectrum (400−1064
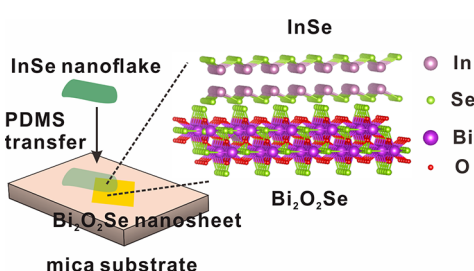
nm) photodetection at zero bias because of the narrow bandgap between the InSe nanoflake and the Bi_2O_2Se nanosheet, theoretical type II band alignment, and a built-in electric field at the high-quality interface. Particularly, a self-powered R of 75.2 mA·W^{-1}, a high $D*$ of 1.08×10^{12} jones, an ultrahigh light on/off ratio over 10^5, and a fast response speed of 5.8/15 ms were achieved under 405 nm irradiation. Additionally, the corresponding R and $D*$ could be further improved at forward bias with the help of the photoconductive effect. Overall, the findings offer great opportunities to design flexible nano-optoelectronics with the merits of low cost, self-driven broadband photoresponse behavior, fast response speed, and robust operational stability. The device may be used in energy-saving, broadband, and highly sensitive photodetectors.

■ RESULTS AND DISCUSSION

The optical image of the as-grown Bi_2O_2Se nanosheets on an F-mica substrate is shown in Figure 1a. In this study, Bi_2O_2Se nanosheets were synthesized using the CVD method under ambient pressure. A schematic of the experimental process has been depicted in Figure S1, and the details have been described in the Experimental Section. Moreover, the Bi_2O_2Se nanosheet/InSe nanoflake heterostructure was prepared via a dry transfer method using polydimethylsiloxane (PDMS). In general, the mechanically exfoliated multilayered InSe flake on PDMS was transferred onto the chosen Bi_2O_2Se nanosheet as illustrated in Figure S2. As shown in Figure 1b, the X-ray diffraction (XRD) pattern of the Bi_2O_2Se nanosheet with lattice planes indexed as (002), (004), and (006) agreed with a previous report,[43] demonstrating the high quality of the synthesized Bi_2O_2Se nanosheet. The images of high-resolution transmission electron microscopy (HRTEM) and patterns of selected-area electron diffraction (SAED) for characterization of the Bi_2O_2Se nanosheet are shown in Figures 1c and 1d. The lattice spacing measured along the (110) plane was 0.28 nm. Additionally, the SAED pattern confirmed the single-crystal nature of the prepared Bi_2O_2Se nanosheet.[40]

Figure 2a illustrates the optical image of the Bi_2O_2Se nanosheet/InSe nanoflake homotype heterostructure device with Cr/Au (5/50 nm) electrodes. The atomic force microscopy (AFM) images of the InSe nanoflake and Bi_2O_2Se nanosheet are shown in Figures 2b and 1c. Additionally, their corresponding height profiles are shown along the red and white dotted lines in Figures 2b and 1c. As a result, the thicknesses of the InSe nanoflake and Bi_2O_2Se nanosheet were identified to be 332 and 7 nm with smooth and clean surfaces, respectively. Moreover, as shown in Figure 2d, the normalized Raman spectra are used to confirm the single crystalline quality and phonon vibration modes of bare InSe, Bi_2O_2Se, and their overlapped region. The Raman peaks of β-InSe at ~116, 177, and 226 cm^{-1} correspond to the vibration modes of out-of-plane A_{1g}^1, in-plane E_{2g}^1, and out-of-plane A_{1g}^2, respectively.[51] Particularly, the representative Raman peak of Bi_2O_2Se located at 159 cm^{-1} is correlated to the out-of-plane A_{1g} vibration, indicating a high single crystalline degree of the CVD-grown sample.[52] All the characteristic peaks without obvious shifts were observed in the overlapped region, indicating a high interfacial quality of the heterostructure after the transfer process. The optical bandgap of the individual InSe and the interlayer coupling of the heterostructure were verified using the PL measurements. As shown in Figure 2e, β-InSe had an asymmetric PL emission peak at ~988 nm, corresponding

Scheme 1. Left: Fabrication Process of the Homo-Type Heterostructure via PDMS Transfer Method; Right: Crystal Structures of InSe and Bi_2O_2Se
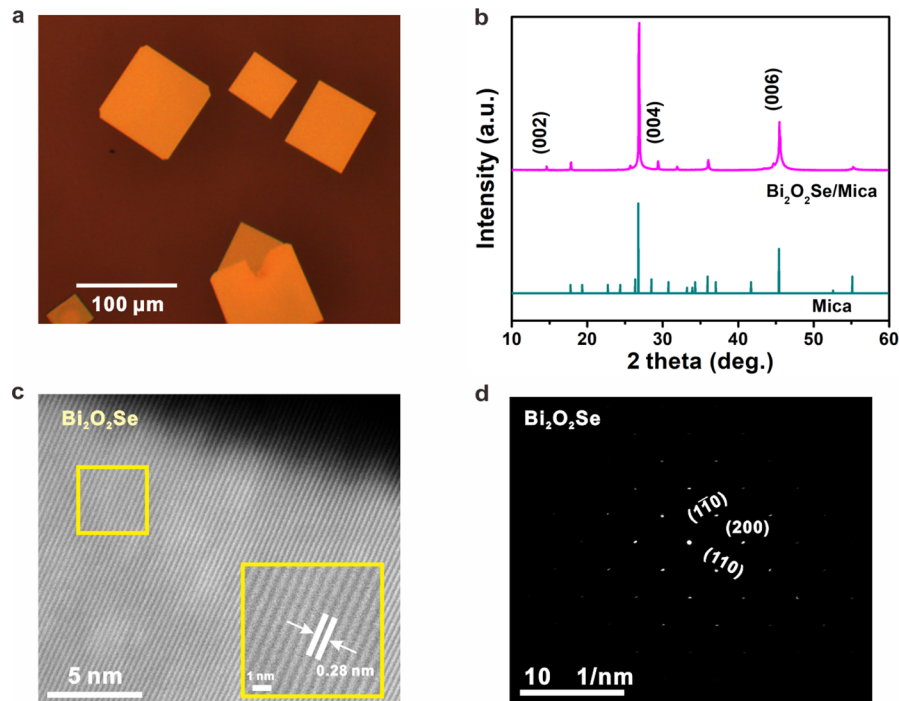
Figure 1. Characterization of the Bi$_2$O$_2$Se nanosheet. (a) Optical image of the as-grown Bi$_2$O$_2$Se nanosheet on F-mica substrate. The scale bar is 100 μm. (b−d) XRD, HRTEM image, and SAED pattern of the Bi$_2$O$_2$Se nanosheet.
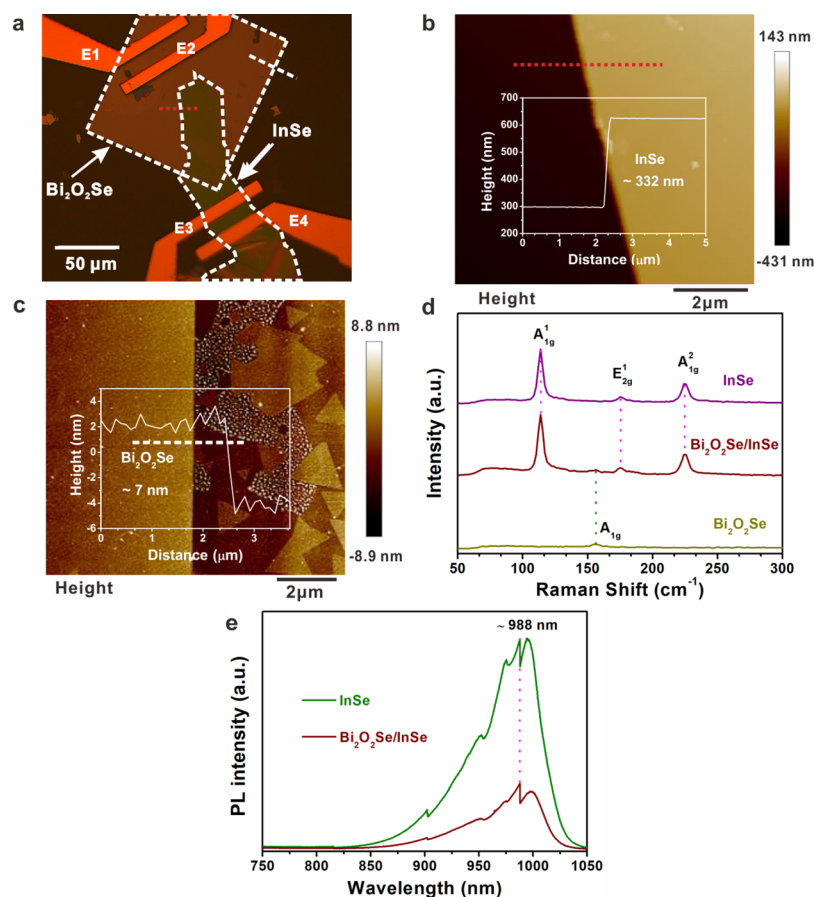
Figure 2. Characterization of the Bi$_2$O$_2$Se nanosheet/InSe nanoflake heterostructure. (a) Optical image of the devices. The scale bar is 50 μm. (b, c) AFM images of InSe and Bi$_2$O$_2$Se nanosheet, respectively. (d) Raman spectra of the overlapping region, bare InSe, and Bi$_2$O$_2$Se nanosheet. (e) PL spectra of individual InSe nanosheet and the Bi$_2$O$_2$Se nanosheet/InSe nanoflake heterostructure.

to the direct optical bandgap at ~1.25 eV.[53] However, the PL intensity was suppressed without a shift for the overlapped region compared to the bare InSe. Hence, this PL quenching effect indicates a rapid efficient separation of the photogenerated electron−hole pairs and decreased PL radiative recombination, resulting in the improvement in the optoelectrical performance of the Bi_2O_2Se nanosheet/InSe nanoflake heterostructure.[54]

As shown in Figure 3a, the measured surface potential difference (SPD) between InSe and Bi_2O_2Se on F-mica was
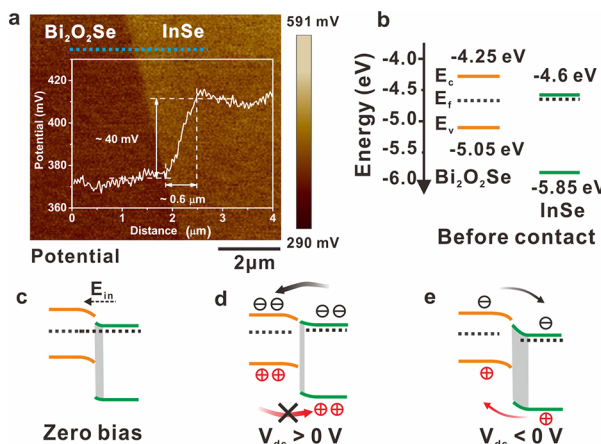

Figure 3. KPFM measurement and energy band arrangement of the Bi_2O_2Se nanosheet/InSe nanoflake heterostructure. (a) KPFM image and the surface contact potential difference between Bi_2O_2Se and InSe nanosheet. (b) Band arrangement of Bi_2O_2Se and InSe nanosheet before contact. (c−e) Band diagrams at zero bias (c), $V_{ds} > 0$ (d), and $V_{ds} < 0$ (e) in the dark.

~40 mV with a lateral depletion width of ~0.6 μm along the blue dashed line, which was obtained using a Kelvin probe force microscope (KPFM). Furthermore, it unveiled an effective built-in electric field pointing from InSe to Bi_2O_2Se across the heterointerface. Accordingly, the theoretical band alignment of the Bi_2O_2Se nanosheet/InSe nanoflake before contact is shown in Figure 3b.[38,48] The conduction band minimum (CBM) values for the Bi_2O_2Se nanosheet and InSe nanoflake were approximately −4.25 and −4.6 eV, respectively, resulting in a small CBM band offset of 0.35 eV. Additionally, the valence band maximum (VBM) values for the Bi_2O_2Se nanosheet and InSe nanoflake were approximately −5.05 and −5.85 eV, respectively, resulting in a large VBM band offset of 0.8 eV. The PL quenching effect of the Bi_2O_2Se nanosheet/InSe nanoflake heterostructure is attributed to the type II band arrangement, which facilitates the generation and separation of photogenerated carriers under laser illumination. As shown in Figure 3c, because InSe has a higher Fermi level than that Bi_2O_2Se, the electrons tend to diffuse from InSe to Bi_2O_2Se after contact, accumulating positive and negative charge centers at the InSe and Bi_2O_2Se sides, respectively. Thus, the band edges at InSe and Bi_2O_2Se bend upward and downward, respectively. Hence, a depletion region is formed at their interface, and the Fermi level becomes equal.[55] Therefore, InSe and Bi_2O_2Se were reported to connect to the source and drain terminals, respectively. As shown in Figures 3d and 3e, the transport process in the dark is highly related to the barrier height of the bias-modulation potential. When drain−source voltage (V_{ds}) > 0 V, the direction of V_{ds} is opposite to the built-

in electric field, leading to a decreased potential barrier height. Owing to the low potential barrier height of the junction, the electrons at the CBM of InSe can be effectively driven across the small band offset and contribute to the electron-dominated forward diffusion current. However, the holes in Bi_2O_2Se are difficult to transmit across the junction owing to the large VBM band offset. On the contrary, when $V_{ds} < 0$, electrons in Bi_2O_2Se are driven to the InSe side without any potential barrier height while minority holes in the InSe side can drift back easily to the Bi_2O_2Se side. Meanwhile, the transmission process of the charge carriers is limited owing to increased depletion strength, leading to an ultralow backward drift current.[38]

Figure 4a illustrates a three-dimensional (3D) schematic diagram of the photodetector based on the Bi_2O_2Se nanosheet/InSe nanoflake under different illumination conditions. The linear drain−source current−voltage ($I_{ds}-V_{ds}$) curves of the Bi_2O_2Se nanosheet and the InSe nanoflake exhibited Ohmic contacts, as shown in Figures S3a and 3b, respectively. As shown in Figures S3c and S3d, the N-type transfer curves of the Bi_2O_2Se nanosheet and InSe nanoflake confirm the N−N homotype heterojunction of the photodetector. The photoresponse properties of the Bi_2O_2Se nanosheet and the InSe nanoflake are shown in Figures S4 and S5, respectively. Moreover, the conductivity of Bi_2O_2Se is considerably much higher than that of InSe, resulting in a unilateral depletion region. As shown in Figure S6, the diode exhibited a forward rectification behavior with an approximate rectification ratio of 2.3×10^2. The rectification behavior is determined based on the depletion region. Furthermore, the ideality factor (n) of the heterostructure is extracted from the Shockley diode equation, which is expressed as follows:[56] $I_{ds} = I_s(e^{qV_{ds}/nk_BT} - 1)$, where I_s represents the reverse saturation current, q represents the electron charge, k_B is the Boltzmann constant, and T is the absolute temperature. The calculated ideality factor was about 1.19 (close to 1) in the 0−0.3 V range, indicating the domination of diffusion current in the forward direction and high-quality interface.[38] Moreover, the $I_{ds}-V_{ds}$ curves at the semilogarithmic scale in the range of −1 to 1 V in the dark and under broadband light illumination are shown in Figure 4b. As expected, the device exhibited an obvious photovoltaic effect characterized with a positive open−circuit voltage (V_{oc}) and a negative short−circuit current (I_{sc}) in a wide spectral range of 405−1064 nm. In particular, the photoresponse behavior at wavelengths >990 nm may be ascribed to the light absorption by the narrow bandgap of Bi_2O_2Se and the effective built-in electric field with type II band alignment. The photoconductive effect could also be achieved in the forward and negative bias regions, leading to high photoresponsivity and specific detectivity.

Furthermore, Figure 4c illustrates the time-resolved curves under light irradiation ranging from visible to near-infrared wavelength at a V_{ds} of 0 V. The fast and stable switching on−off curves confirm a fast and broadband spectral operation in a self-driven mode. Specifically, as shown in Figure S7, the photoresponse times of the self-powered Bi_2O_2Se nanosheet/InSe nanoflake homotype heterojunction device at the wavelengths of 635 nm (26.27 mW·cm^{-2}), 808 nm (49.3 mW·cm^{-2}), 980 nm (27.3 mW·cm^{-2}), and 1064 nm (42.7 mW·cm^{-2}) are estimated to be approximately 47.6/27.3, 46.6/51.9, 37.6/31.5, and 297.2/328 ms, respectively. Furthermore, a detailed discussion of the photoresponse properties of the
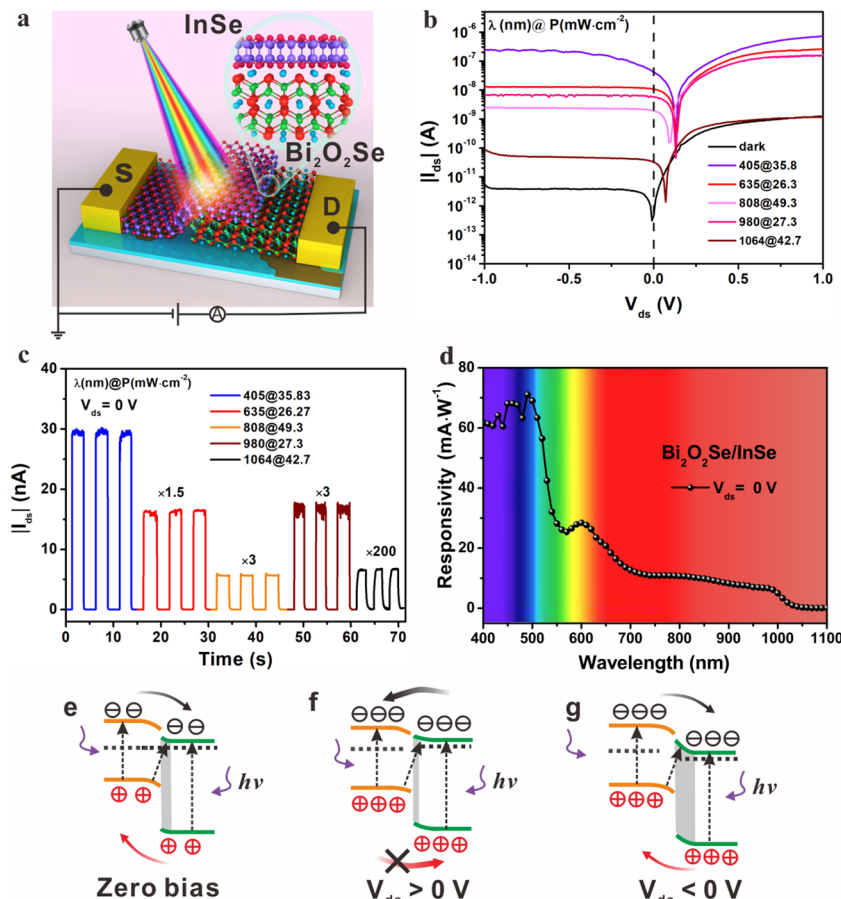
Figure 4. Self-powered broadband photodetection performance of the Bi_2O_2Se nanosheet/InSe nanoflake heterostructure diode. (a) 3D schematic image of the device under broadband light illumination. (b) $I_{ds}-V_{ds}$ curves in dark and under various light irradiations. (c) Time-resolved I_{ds} curves under 405, 635, 808, 980, and 1064 nm illumination. (d) Responsivity as a function of wavelength from 400 to 1100 nm. Schematic energy band diagram and transport mechanism under light irradiation (e) at V_{ds} = 0 V, (f) V_{ds} > 0 V, and (g) V_{ds} < 0 V.

device at 405 and 980 nm will be presented later. The broadband photocurrent spectrum without an external bias and the corresponding incident light power spectrum in the 400−1100 nm range are presented in Figure S8a,b. The photodetector exhibited an obvious broadband and zero-bias photoresponse in the 400−1100 nm range, as shown in Figure 4d. The maximum R is calculated to be 71 mA·W^{-1} based on the equation of R_λ. Therefore, the optimal wavelength is ∼490 nm. With the longer incident light wavelength, the lower photon energy results in a decreased light absorption coefficient and a decrease in the value of R. The transport mechanism of the photogenerated carriers with and without external biases is discussed herein. Under visible and near-infrared light illumination from 400 to 988 nm ($h\nu > E_g(InSe)$ and $E_g(Bi_2O_2Se)$), the band structures of InSe and Bi_2O_2Se can excite the photons and be separated by the built-in electric field of 40 meV (gray region). As shown in Figure 4e, at zero bias, the photogenerated electrons located at the CBM of Bi_2O_2Se can be drifted to the CBM of InSe while the holes at the VBM of InSe can easily transmitted to the VBM of Bi_2O_2Se, leading to a positive V_{oc} and a negative I_{sc}. Moreover, an intralayer transition can occur at the small band offset of 0.45 eV, leading to a photoresponse at the longer wavelength. Under near-infrared light >988 nm, the band structure of Bi_2O_2Se can primarily excite the photons, resulting in a low photocurrent in the circuit. When the external electric field is applied, the potential barrier height can be effectively

modulated. As shown in Figure 4f, when V_{ds} > 0, the built-in potential barrier region (gray region) can be reduced. The photogenerated electrons at the CBM of InSe can be drifted and transported to the CBM of Bi_2O_2Se through the small CBM band offset of 0.35 eV. In contrast, most of the holes at the VBM of Bi_2O_2Se find it difficult to cross the large VBM band offset of 0.8 eV. Therefore, the diffusion photocurrent in the forward bias region is dominated by the electrons in InSe. As shown in Figure 4g, when V_{ds} < 0, the built-in potential barrier can be increased, resulting in an ultralow dark current of 5.5 pA. The photogenerated electrons at the CBM of Bi_2O_2Se can easily drift to the CBM of InSe at a large built-in electric field. At the same time, the photogenerated holes at the VBM of InSe can also drift to the Bi_2O_2Se side. Thus, the drift photocurrent in the backward bias region is dominated by the entire heterojunction. In brief, the experimental results and the theoretical analysis indicate that the fabricated Bi_2O_2Se nanosheet/InSe nanoflake homotype heterostructure can serve as a fast and stable self-driven photodetector in the entire range of −1 to 1 V.

Figure 5a shows the $I_{ds}-V_{ds}$ curves of the heterostructure in the dark condition and under 405 nm laser illumination at different light power densities on a semilogarithmic scale. The generation of photocurrent can be seen at a V_{ds} of 0 and ±1 V. As shown in Figure S9a, the V_{oc} and I_{sc} extracted from Figure 5a increase with light power density, with maximum values of 0.15 V and 67.45 nA, respectively, under the illumination
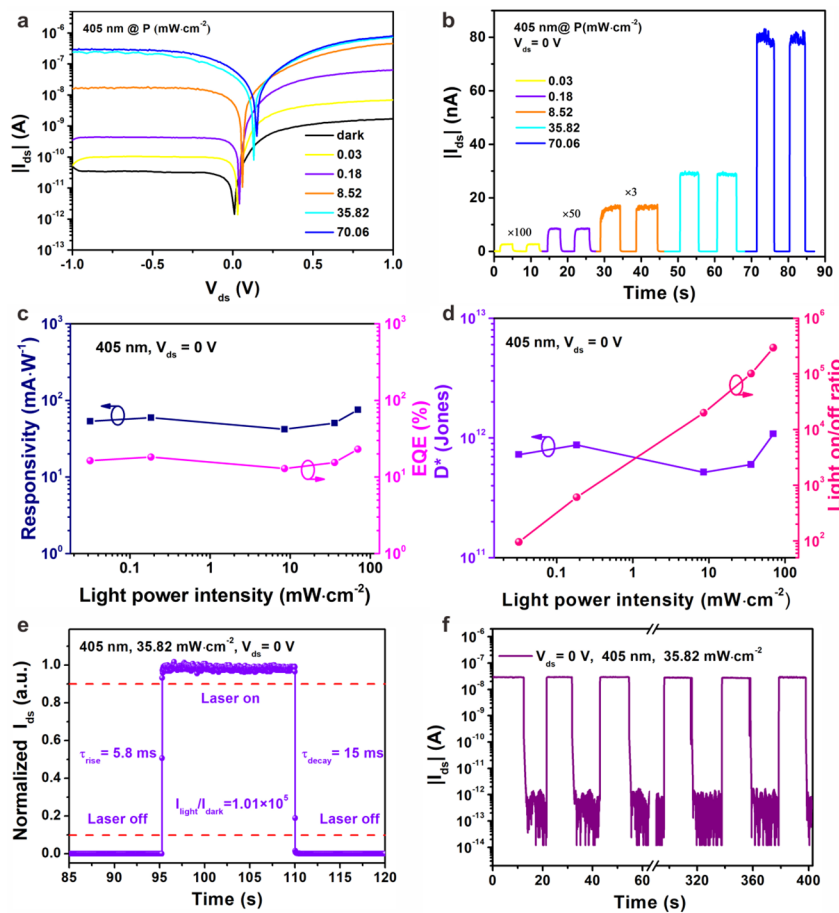
Figure 5. Self-driven photodetection performance of the Bi_2O_2Se nanosheet/InSe nanoflake heterostructure device under 405 nm light illumination. (a) $I_{ds}-V_{ds}$ curves of the device in dark and under 405 nm light illumination with increasing light power densities. (b) Time-resolved switching on−off curve with increasing light power densities. (c, d) R, EQE, $D*$, and light on/off ratio of the photodetector as a function of light power density. (e) Time-resolved I_{ds} with switching on−off at P = 35.82 mW·cm^{-2}. (f) Time-resolved curve in 20 cycles.

intensity of 70.06 mW·cm^{-2}. Moreover, I_{sc} and the light power intensity (P) can be fitted using a power law equation: $I_{ph} \propto P^{\alpha}$. The obtained value of the fitting exponent α was 0.87 (close to 1). The sublinear exponent indicates the existence of defects, impurities, or adsorbed molecule-induced trap states across the heterostructure, leading to the incomplete photo-electric conversion.[39] Furthermore, the photogenerated output electric power (P_{el}) can be extracted using the formula $P_{el} = I_{ds} \times V_{ds}$.[38] As shown in Figure S9b, P_{el}, as a function of V_{ds}, is plotted under varied P. P_{el} reached a maximum value of 2.13 nW at a P of 70.06 mW·cm^{-2}. Furthermore, the fill factor (FF) is an important parameter indicating the photovoltaic conversion efficiency in solar cells and is defined as follows: FF = $P_{el,max}/(I_{sc} \times V_{oc})$.[38] As shown in Figure S10, a maximum FF of 0.33 is obtained at a P of 0.03 mW·cm^{-2}. Moreover, power conversion efficiency (PCE), another figure of merit of a photovoltaic device, is defined as follows: PCE = P_{el}/P_{in}.[38] The calculated maximum PCE was 0.9% at a P of 35.82 mW·cm^{-2}, as shown in Figure S10. Furthermore, the maximum values of FF and PCE of the photodetector based on the Bi_2O_2Se nanosheet/InSe nanoflake photodetector are comparable to a previously reported photodetector based on a Bi_2O_2Se-based heterostructure.

Furthermore, the time-resolved switching of on−off curves with different laser densities at V_{ds} = 0 and ±1 V are shown in Figures 5b, S11c, and S12. The photocurrent values are

consistent with the results in Figure 5a. Moreover, stable and reproducible characteristics are achieved for the homotype photodiode designed in this study. Typically, responsivity R_{λ}, external quantum efficiency (EQE), $D*$, response speed, and I_{light}/I_{dark} ratio are critical figures of merit, which evaluate the performance of a photodetector. In general, R_{λ} is used to characterize photoresponsivity, which is defined as follows: $R_{\lambda} = \frac{I_{ph}}{SP} = \frac{I_{illumination} - I_{dark}}{SP}$, where I_{ph} is the net photocurrent, $I_{illumination}$ is the I_{ds} under light illumination, I_{dark} is the I_{ds} in the dark condition, and S is the effective area.[57] The overlapped region of the Bi_2O_2Se nanosheet/InSe nanoflake hetero-structure is approximately 1560 μm^2. Moreover, EQE, which describes the ratio of the number of photogenerated carriers to that of the incident photons, is defined as follows: EQE = $\frac{hcR_{\lambda}}{e\lambda}$, where h is the Planck constant (6.626×10^{-34} J·s), c is the speed of light (3.0×10^8 m·s^{-1}), e is the elementary charge (1.6×10^{-19} C), and λ is the incident light wavelength.[58]

Additionally, $D*$ represents the ability of a photodetector to detect a weak light signal and can be expressed as follows: $D* = \frac{R_{\lambda}\sqrt{S}}{\sqrt{2eI_{dark}}}$.[58] The R, EQE, and $D*$ of the Bi_2O_2Se nanosheet/InSe nanoflake heterostructure photodetector, as a function of P, are shown in Figure 5c,d. The values of R, EQE, and $D*$ fluctuate within a certain range of 42.0−75.24 mA·W^{-1}, 12.87%−23.05%, and 5.17×10^{11}−1.08×10^{12} jones,
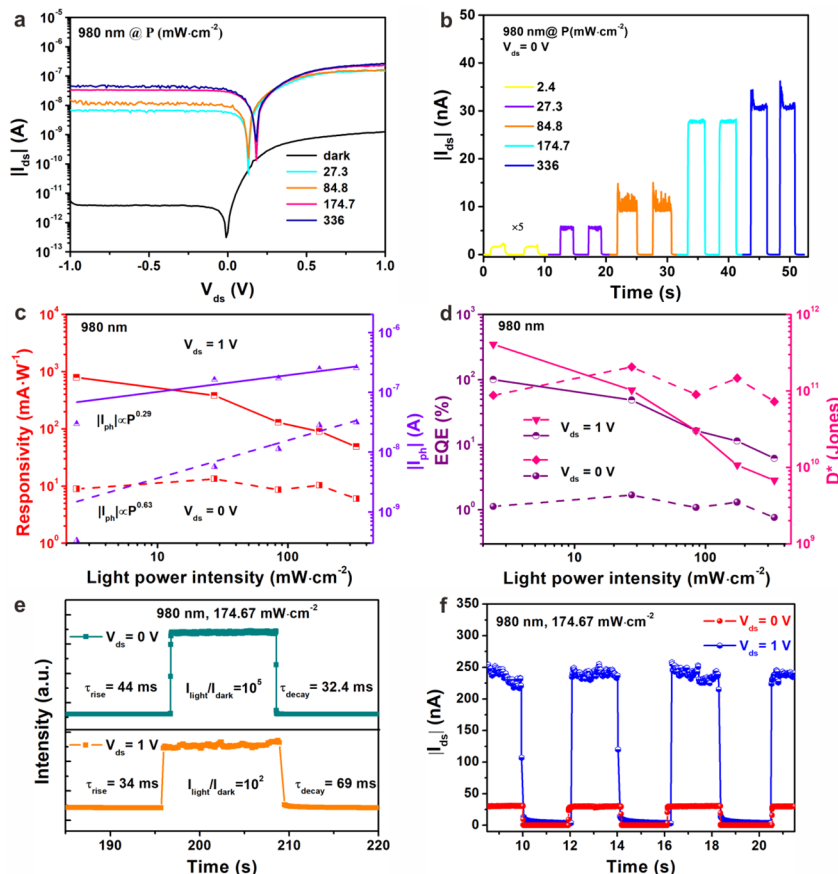
Figure 6. Photoresponse characteristics of the Bi_2O_2Se nanosheet/InSe nanoflake heterostructure photodetector under 980 nm laser illumination. (a) $I_{ds}-V_{ds}$ curves of the photodetector in the dark and under 980 nm light irradiation with different light power intensities. (b) Time-resolved switching on−off curves with increasing light power intensities. (c, d) Net photoresponsivity, photocurrent, EQE, and D^* of the photodetector varying with incident laser intensities under $V_{ds} = 0$ V (dashed lines) and $V_{ds} = 1$ V (solid lines). (e, f) Time-dependent I_{ds} and on−off photoresponse of the heterostructure based photodetector under light power intensity of 174.67 mW·cm^{-2} with 0 and 1 V bias voltages, respectively.

respectively, within the entire range of light power density. The maximum photovoltaic R, EQE, and D^* values of 75.2 mA· W^{-1}, 23%, and 1.08×10^{12} jones at a P of 70 mW·cm^{-2}, respectively, are obtained under 405 nm laser illumination. This is because the photogenerated carriers at the high quality interface (the ideality factor of 1.19) with few recombination centers (α value of 0.87, which is close to 1) contribute to the efficient photoelectric conversion under the type II band alignment at high light density. Furthermore, R, EQE, and D^* can be further enhanced to their maximum values of 13.6 A· W^{-1}, 4.16×10^3%, and 4.24×10^{12} jones, respectively, at a P of 0.18 mW·cm^{-2} and V_{ds} of 1 V, as shown in Figure S11a,b. The I_{light}/I_{dark} ratio at a V_{ds} of 0 V is considerably enhanced from 10^2 to 3×10^5 with the increment in P from 0.03 to 70 mW· cm^{-2}. This is because the large photogenerated electron−hole pairs are separated by the built-in electric field through the type II band alignment at high light power density. Meanwhile, an ultralow dark current of 0.28 pA is maintained in the depletion region. As shown in Figures 5e and S11d, the response speed at V_{ds} of 0 and 1 V is characterized by rise time, τ_{rise} (time needed for I_{ds} to rise from 10% to 90% of the maximum I_{ds}), and decay time, τ_{decay} (time needed for I_{ds} to drop from 90% to 10% of the maximum I_{ds}), which is calculated to be 5.8/15 m/s and 37.2/91 m/s, respectively, at a P of 35.82 mW·cm^{-2}. The long decay time or recombination rate may be attributed to the defect states induced by the

environmental molecules, such as oxygen and water, across the interface.[59] In addition, Figure 5f illustrates the self-driven switching on−off behavior with negligible deviation over 400 s, indicating the repeatability and stability of the fabricated device at zero bias.

The development of high-performance near-infrared photo-detectors is of great importance for industry and communication. To ensure minimum damage and adequate safety of fiber components, a large number of photodetectors are equipped with a system of high-power fiber lasers using laser diodes at the near-infrared wavelengths of 915 and 976 nm[60] as the pumping sources. Herein, the performances of the photodetector based on Bi_2O_2Se nanosheet/InSe nanoflake in the near-infrared region are also discussed. Figure 6a shows the I−V curves of the device under the dark condition and under 980 nm laser illumination with different P at the semilogarithmic scale. Furthermore, the time-resolved switching on−off curves of the device with increasing P were measured, as shown in Figure 6b. Moreover, R, I_{ph}, EQE, and D^* of the device, as a function of P under 980 nm laser illumination at V_{ds} of 0 and 1 V are shown in Figures 6c and 6d, respectively. When $P = 2.4$ mW·cm^{-2}, R reaches a value of 790 mA·W^{-1}/8.87 mA·W^{-1} at V_{ds} of 1 V/0 V. Moreover, the values of α values at V_{ds} of 0 and 1 V were calculated to be approximately 0.63 and 0.29, respectively, indicating the existence of high gain and photogating under an external

field.[38] As illustrated in Figure 6d, the maximum EQE and D^* values of 100%/1.68% and 4.07×10^{11} jones/2.06×10^{11} jones are obtained at V_{ds} of 1 and 0 V, respectively. In addition, Figure 6e displays the time-dependent photoresponse under 980 nm light illumination at a P of 174.67 mW·cm^{-2} and a V_{ds} of 1 and 0 V. The device exhibits a fast response with τ_{rise} of 34 and 44 ms and τ_{decay} of 69 and 32.4 ms at V_{ds} of 1 and 0 V, respectively. On the other hand, owing to the suppressed dark current, the self-powered photodetector shows a large I_{light}/I_{dark} ratio of 10^5 compared to 10^2 at a V_{ds} bias of 1 V. The corresponding fast and stable photoresponse behaviors are also shown in Figure 6f. Additionally, the photoelectric conversion performance under 980 nm light illumination is shown in Figure S13. The maximum values of P_{el}, FF, and PCE are ~1.75 nW, 0.4, and 0.067%, respectively. Moreover, the self-powered photoresponse properties under 1064 nm light illumination (Bi_2O_2Se domination) are illustrated in Figure S14, which demonstrates moderate photoresponse having a τ_{rise} of 307.2 ms, a τ_{decay} of 217.4 ms, a high I_{light}/I_{dark} ratio of 10^3, and robust repeatability. Furthermore, the figures of merit affecting the photodetection performance of the photodetectors based on the proposed Bi_2O_2Se nanosheet/InSe nanoflake and previously reported Bi_2O_2Se nanosheet-based 2D heterostructure are listed in Table S1.

CONCLUSION

Herein, a homotype CVD-grown photodetector based on the Bi_2O_2Se nanosheet/InSe nanoflake vdW heterojunction is successfully fabricated. First, a rectification ratio of 2.3×10^2 can be achieved owing to the high quality heterointerface. The photovoltaic and photoconductive effects enable the device to act as an excellent, self-powered photodetector ranging from visible (400 nm) to near-infrared (1064 nm) wavelengths under a tunable built-in electric field using the designed type II band alignment. Moreover, the synergistic effect comprising the high light absorption coefficiency, direct bandgap of multilayered InSe nanoflake, high carrier mobility, and broadband photoresponse of the Bi_2O_2Se nanosheet contributed to the high optoelectrical performance of the photodetector in the V_{ds} range of −1 to 1 V. The fast photoresponse, high photosensitivity, and ultrahigh I_{light}/I_{dark} ratio of the self-powered photodetector based on 2D the Bi_2O_2Se nanosheet/InSe nanoflake heterostructure has potential application in self-driven photodetectors, photodiodes, imaging sensors, and rectifiers.

EXPERIMENTAL SECTION

Preparation of Few-Layer Bi_2O_2Se Nanosheets. Bi_2O_2Se nanosheets were synthesized via the CVD method under ambient pressure. The schematic of the experimental setup is illustrated in Figure S1. First, 150 mg of Bi_2Se_3 powder and 450 mg of Bi_2O_3 powder were poured onto quartz boats and placed in a quartz tube, where Bi_2Se_3 was located at the upper stream region about 2−3 cm away from the edge of the single temperature zone tubular furnace and Bi_2O_3 was located at the middle area (9−11 cm away from the upstream edge of the furnace) of the furnace. Subsequently, four freshly cleaved mica substrates (mica, 10 mm × 10 mm × 0.2 mm, purchased from Tebo Technology Co., Ltd.) arranged as an array (2 × 2) were placed onto a piece of mechanically cleaved SiO$_2$/Si substrate in rectangular shape (2.2 cm × 4 cm). Then, SiO$_2$/Si substrate together with arrayed mica substrates were placed at downstream, where the middle of the mica array was located at 22 cm referenced by the upstream edge of the furnace. Note that the freshly cleaved mica substrate plays a vital role in growing large scale Bi_2O_2Se

nanosheet, which can be simply obtained by the assistance of tweezers. Furthermore, the mica substrates arranged as an array could improve the probability in growth of large-size few-layer Bi_2O_2Se nanosheets. Next, the quartz tube was sealed and flushed by Ar gas with a high flow rate for 10 min to eliminate the air atmosphere. After that, the flow rate of Ar gas was set to be 200 sccm. The growth temperature was set to be 700 °C under environmental pressure with a ramp time of 60 min and held for 150 min. Finally, the furnace was naturally cooled to room temperature. Besides, we also find that the Bi_2Se_3 and Bi_2O_3 remaining in the quartz tube could be reused for several times on epitaxial growth of 2D Bi_2O_2Se nanosheets.

Fabrication of the Bi_2O_2Se Nanosheet/InSe Nanoflake Heterostructure Device. The Bi_2O_2Se nanosheet/InSe nanoflake heterostructure was fabricated via a PDMS (17 mil, Gel Pak) assisted all dry transfer method with merits of cleanliness, high quality interface, and simple operation. The schematic diagram of the heterostructure fabrication process is displayed in Figure S2. The InSe nanoflake with chosen thickness was preciously transferred and vertically stacked on Bi_2O_2Se nanosheet on mica substrate via a 2D material transfer platform (Shanghai OnWay Technology Co., Ltd.) equipped with an optical microscope. Then, contact electrodes (Ni/Au, 5/50 nm) of the device were obtained using an ultraviolet lithography technology (TuoTuo Technology Co., Ltd.) and electron-beam evaporation (Anhui Jiashuo Vacuum Technology Co., Ltd.).

Characterization and Measurements. An optical microscope (Motic Moticcam Pro 205A) was used to capture the optical images. The thickness of the InSe nanosheet and Bi_2O_2Se thin flake was measured via atomic force microscopy (AFM) (Dimension FastScan, Bruker Co., Ltd.). Raman and PL spectra (Nost Technology Co., Ltd.) were recorded at room temperature equipped with a 50 W, 532 nm laser. The electrical and photoresponse behaviors of the device were tested using a four-probe station (PSAICPB6A, Precision Systems Industrial Co., Ltd.) connected with a semiconductor analyzer system (Keithley 2636B). The light source ranging from 400 to 1100 nm was provided via a broadband bromine tungsten lamp. The photoresponse performances of the device were measured under an ambient atmosphere using lasers with wavelengths of 405 and 635 nm with spot diameters of 4 mm and wavelengths of 808, 980, and 1064 nm with spot sizes of 5 mm × 1.5 mm. The photoresponse times were extracted using a chopper controlled by modulated functions.

ASSOCIATED CONTENT

Ⓢ **Supporting Information**

The Supporting Information is available free of charge at https://pubs.acs.org/doi/10.1021/acsanm.3c00054.

Details about the schematic diagram of the experimental setup for preparation of Bi_2O_2Se nanosheets; schematic diagram of the PDMS assisted dry transfer process of Bi_2O_2Se nanosheet/InSe nanoflake heterostructure; $I_{ds}−V_{ds}$ and transfer curve of bare Bi_2O_2Se nanosheet and InSe nanosheet; photoresponse properties of individual Bi_2O_2Se nanosheet; photoresponse properties of individual InSe nanoflake; $I_{ds}−V_{ds}$ curves of the Bi_2O_2Se nanosheet/InSe nanoflake heterojunction device in linear and semilogarithmic scale; photoresponse time of the self-powered Bi_2O_2Se nanosheet/InSe nanoflake homotype heterojunction device in broadband spectral; broadband photocurrent spectrum of the Bi_2O_2Se nanosheet/InSe nanoflake heterostructure device without external bias; corresponding incident light power density spectrum ranging from 400 to 1100 nm; V_{oc} and I_{sc} of the Bi_2O_2Se nanosheet/InSe nanoflake device versus light power intensity; output electrical power as a function of V_{ds} at various light power densities under 405 nm; FF and PCE of the heterostructure device as a function of laser power intensity; photoresponse

performance of the Bi_2O_2Se nanosheet/InSe nanoflake photodetector under 405 nm light illumination at V_{ds} = 1 V; time-resolved I_{ds} curves of the device under 405 nm light with various light power densities at V_{ds} = −1 V; photoelectric conversion performance of the device under 980 nm light illumination; self-powered photoresponse properties of the Bi_2O_2Se nanosheet/InSe nanoflake photodetector under 1064 nm light illumination; figure of merits of photodetection performance of Bi_2O_2Se nanosheet-based 2D/2D heterostructures (PDF)

■ AUTHOR INFORMATION

Corresponding Authors

Wei Gao − Guangdong Provincial Key Laboratory of Chip and Integration Technology, School of Semiconductor Science and Technology, South China Normal University, Foshan 528225, P. R. China; ◎ orcid.org/0000-0002-8159-3957; Email: gaowei317040@m.scnu.edu.cn

Jingbo Li − Guangdong Provincial Key Laboratory of Chip and Integration Technology, School of Semiconductor Science and Technology, South China Normal University, Foshan 528225, P. R. China; Email: jbli@m.scnu.edu.cn

Authors

Zhiyang Zhang − Guangdong Provincial Key Laboratory of Chip and Integration Technology, School of Semiconductor Science and Technology, South China Normal University, Foshan 528225, P. R. China

Lixiang Han − Guangdong Provincial Key Laboratory of Chip and Integration Technology, School of Semiconductor Science and Technology, South China Normal University, Foshan 528225, P. R. China

Zhiying Dan − Guangdong Provincial Key Laboratory of Chip and Integration Technology, School of Semiconductor Science and Technology, South China Normal University, Foshan 528225, P. R. China; Faculty of Science and Engineering, University of Groningen, Groningen 003150, Netherlands

Hengyi Li − Guangdong Provincial Key Laboratory of Chip and Integration Technology, School of Semiconductor Science and Technology, South China Normal University, Foshan 528225, P. R. China

Mengmeng Yang − Guangdong Provincial Key Laboratory of Chip and Integration Technology, School of Semiconductor Science and Technology, South China Normal University, Foshan 528225, P. R. China

Yiming Sun − Guangdong Provincial Key Laboratory of Chip and Integration Technology, School of Semiconductor Science and Technology, South China Normal University, Foshan 528225, P. R. China

Zhaoqiang Zheng − College of Materials and Energy, Guangdong University of Technology, Guangzhou 510006, P. R. China; ◎ orcid.org/0000-0002-1699-2425

Nengjie Huo − Guangdong Provincial Key Laboratory of Chip and Integration Technology, School of Semiconductor Science and Technology, South China Normal University, Foshan 528225, P. R. China; ◎ orcid.org/0000-0003-2520-6243

Dongxiang Luo − Huangpu Hydrogen Innovation Center/ Guangzhou Key Laboratory for Clean Energy and Materials, School of Chemistry and Chemical Engineering, Guangzhou University, Guangzhou 510006, P. R. China

Complete contact information is available at:

Author Contributions

J.B.L. designed the project; W.G. and Z.Y.Z. performed the experiments; L.X.H. synthesized the Bi_2O_2Se nanosheets, drew the figures, and wrote the manuscript with the help from W.G. and N.J.H.; other authors discussed the results.

Author Contributions

Z.Z. and L.H. contributed equally to this work.

Notes

The authors declare no competing financial interest.

■ ACKNOWLEDGMENTS

■ REFERENCES

(1) Novoselov, K. S.; Geim, A. K.; Morozov, S. V.; Jiang, D.; Zhang, Y.; Dubonos, S. V.; Grigorieva, I. V.; Firsov, A. A. Electric field effect in atomically thin carbon films. Science 2004, 306 (5696), 666−669.

(2) Schaibley, J. R.; Yu, H. Y.; Clark, G.; Rivera, P.; Ross, J. S.; Seyler, K. L.; Yao, W.; Xu, X. D. Valleytronics in 2D materials. Nat. Rev. Mater. 2016, 1 (11), 16055.

(3) Gupta, A.; Sakthivel, T.; Seal, S. Recent development in 2D materials beyond graphene. Prog. Mater. Sci. 2015, 73, 44−126.

(4) Cao, Y.; Fatemi, V.; Fang, S.; Watanabe, K.; Taniguchi, T.; Kaxiras, E.; Jarillo-Herrero, P. Unconventional superconductivity in magic-angle graphene superlattices. Nature 2018, 556 (7699), 43−50.

(5) Novoselov, K. S.; Jiang, Z.; Zhang, Y.; Morozov, S. V.; Stormer, H. L.; Zeitler, U.; Maan, J. C.; Boebinger, G. S.; Kim, P.; Geim, A. K. Room-temperature quantum hall effect in graphene. Science 2007, 315 (5817), 1379−1379.

(6) Huo, N. J.; Konstantatos, G. Recent Progress and Future Prospects of 2D-Based Photodetectors. Adv. Mater. 2018, 30 (51), 1801164.

(7) Zou, Z. X.; Liang, J. W.; Zhang, X. H.; Ma, C.; Xu, P.; Yang, X.; Zeng, Z. X. S.; Sun, X. X.; Zhu, C. G.; Liang, D. L.; Zhuang, X. J.; Li, D.; Pan, A. L. Liquid-Metal-Assisted Growth of Vertical GaSe/MoS_2 p-n Heterojunctions for Sensitive Self-Driven Photodetectors. ACS Nano 2021, 15 (6), 10039−10047.

(8) Gao, W.; Zhang, F.; Zheng, Z. Q.; Li, J. B. Unique and Tunable Photodetecting Performance for Two-Dimensional Layered $MoSe_2$/WSe_2 p-n Junction on the 4H-SiC Substrate. ACS Appl. Mater. Interfaces 2019, 11 (21), 19277−19285.

(9) Yang, M. M.; Gao, W.; He, M. J.; Zhang, S.; Huang, Y.; Zheng, Z. Q.; Luo, D. X.; Wu, F. G.; Xia, C. X.; Li, J. B. Self-driven $SnS_{1-x}Se_x$ alloy/GaAs heterostructure based unique polarization sensitive photodetectors. Nanoscale 2021, 13 (36), 15193−15204.

(10) Zhao, Q. X.; Gao, F.; Chen, H. Y.; Gao, W.; Xia, M. J.; Pan, Y.; Shi, H. Y.; Su, S. C.; Fang, X. S.; Li, J. B. High performance polarization-sensitive self-powered imaging photodetectors based on a p-Te/n-$MoSe_2$ van der Waals heterojunction with strong interlayer transition. Mater. Horizons 2021, 8 (11), 3113−3123.

(11) Han, L. X.; Yang, M. M.; Wen, P. T.; Gao, W.; Huo, N. J.; Li, J. B. A high performance self-powered photodetector based on a 1D Te-2D WS_2 mixed-dimensional heterostructure. Nanoscale Adv. 2021, 3 (9), 2657−2665.

(12) Zheng, Z.; Zu, X. T.; Zhang, Y.; Zhou, W. L. Rational design of type-II nano-heterojunctions for nanoscale optoelectronics. Mater. Today Phys. 2020, 15, 100262.

(13) Wang, F. K.; Yang, S. J.; Wu, J.; Hu, X. Z.; Li, Y.; Li, H. Q.; Liu, X. T.; Luo, J. H.; Zhai, T. Y. Emerging two-dimensional bismuth oxychalcogenides for electronics and optoelectronics. *InfoMat* **2021**, *3* (11), 1251−1271.

(14) Sun, Y.; Zhang, J.; Ye, S.; Song, J.; Qu, J. L. Progress Report on Property, Preparation, and Application of Bi_2O_2Se. *Adv. Funct. Mater.* **2020**, *30* (49), 2004480.

(15) Wu, J. H.; Wei, M. L.; Mu, J. L.; Ma, H.; Zhong, C. Y.; Ye, Y. T.; Sun, C. L.; Tang, B.; Wang, L. C.; Li, J. Y.; Xu, X. M.; Liu, B. L.; Li, L.; Lin, H. T. High-Performance Waveguide-Integrated Bi_2O_2Se Photodetector for Si Photonic Integrated Circuits. *ACS Nano* **2021**, *15* (10), 15982−15991.

(16) Yan, J. M.; Ying, J. S.; Yan, M. Y.; Wang, Z. C.; Li, S. S.; Chen, T. W.; Gao, G. Y.; Liao, F. Y.; Luo, H. S.; Zhang, T.; Chai, Y.; Zheng, R. K. Optoelectronic Coincidence Detection with Two-Dimensional Bi_2O_2Se Ferroelectric Field-Effect Transistors. *Adv. Funct. Mater.* **2021**, *31* (40), 2103982.

(17) Chen, Y. F.; Ma, W. L.; Tan, C. W.; Luo, M.; Zhou, W.; Yao, N. J.; Wang, H.; Zhang, L. L.; Xu, T. F.; Tong, T.; Zhou, Y.; Xu, Y. B.; Yu, C. H.; Shan, C. X.; Peng, H. L.; Yue, F. Y.; Wang, P.; Huang, Z. M.; Hu, W. D. Broadband Bi_2O_2Se Photodetectors from Infrared to Terahertz. *Adv. Funct. Mater.* **2021**, *31* (14), 2009554.

(18) Li, J.; Wang, Z. X.; Wen, Y.; Chu, J. W.; Yin, L.; Cheng, R. Q.; Lei, L.; He, P.; Jiang, C.; Feng, L. P.; He, J. High-Performance Near-Infrared Photodetector Based on Ultrathin Bi_2O_2Se Nanosheets. *Adv. Funct. Mater.* **2018**, *28* (10), 1706437.

(19) Xu, Z. K.; Wang, J. L.; Wang, T.; Hu, W. H.; Yang, X. H.; Lin, X. Huge permittivity and premature metallicity in Bi_2O_2Se single crystals. *Sci. China Phys. Mech. Astron.* **2021**, *64* (6), 267312.

(20) Ge, Z.; Zhao, W.; Yuan, S.; Gao, Z.; Hao, C.; Ma, H.; Ren, H.; Guo, W. Effect of surface Se concentration on stability and electronic structure of monolayer Bi_2O_2Se. *Appl. Surf. Sci.* **2023**, *611*, 155528.

(21) Yang, X.; Zhang, Q.; Song, Y. C.; Fan, Y. S.; He, Y. W.; Zhu, Z. H.; Bai, Z. Q.; Luo, Q.; Wang, G.; Peng, G.; Zhu, M. J.; Qin, S. Q.; Novoselov, K. High Mobility Two-Dimensional Bismuth Oxyselenide Single Crystals with Large Grain Size Grown by Reverse-Flow Chemical Vapor Deposition. *ACS Appl. Mater. Interfaces* **2021**, *13* (41), 49153−49162.

(22) Khan, U.; Luo, Y. T.; Tang, L.; Teng, C. J.; Liu, J. M.; Liu, B. L.; Cheng, H. M. Controlled Vapor Solid Deposition of Millimeter-Size Single Crystal 2D Bi_2O_2Se for High-Performance Photo-transistors. *Adv. Funct. Mater.* **2019**, *29* (14), 1807979.

(23) Kang, M.; Chai, H. J.; Jeong, H. B.; Park, C.; Jung, I. Y.; Park, E.; Cicek, M. M.; Lee, I.; Bae, B. S.; Durgun, E.; Kwak, J. Y.; Song, S.; Choi, S. Y.; Jeong, H. Y.; Kang, K. Low-Temperature and High-Quality Growth of Bi_2O_2Se Layered Semiconductors via Cracking Metal-Organic Chemical Vapor Deposition. *ACS Nano* **2021**, *15* (5), 8715−8723.

(24) Wu, J. X.; Qiu, C. G.; Fu, H. X.; Chen, S. L.; Zhang, C. C.; Dou, Z. P.; Tan, C. W.; Tu, T.; Li, T. R.; Zhang, Y. C.; Zhang, Z. Y.; Peng, L. M.; Gao, P.; Yan, B. H.; Peng, H. L. Low Residual Carrier Concentration and High Mobility in 2D Semiconducting Bi_2O_2Se. *Nano Lett.* **2019**, *19* (1), 197−202.

(25) Chen, C.; Wang, M. X.; Wu, J. X.; Fu, H. X.; Yang, H. F.; Tian, Z.; Tu, T.; Peng, H.; Sun, Y.; Xu, X.; Jiang, J.; Schroter, N. B. M.; Li, Y. W.; Pei, D.; Liu, S.; Ekahana, S. A.; Yuan, H. T.; Xue, J. M.; Li, G.; Jia, J. F.; Liu, Z. K.; Yan, B. H.; Peng, H. L.; Chen, Y. L. Electronic structures and unusually robust bandgap in an ultrahigh-mobility layered oxide semiconductor, Bi_2O_2Se. *Sci. Adv.* **2018**, *4* (9), No. eaat8355.

(26) Zhang, C. C.; Wu, J. X.; Sun, Y. W.; Tan, C. W.; Li, T. R.; Tu, T.; Zhang, Y. C.; Liang, Y.; Zhou, X. H.; Gao, P.; Peng, H. L. High-Mobility Flexible Oxyselenide Thin-Film Transistors Prepared by a Solution-Assisted Method. *J. Am. Chem. Soc.* **2020**, *142* (6), 2726−2731.

(27) Liang, Y.; Chen, Y. J.; Sun, Y. W.; Xu, S. P.; Wu, J. X.; Tan, C. W.; Xu, X. F.; Yuan, H. T.; Yang, L. X.; Chen, Y. L.; Gao, P.; Guo, J. D.; Peng, H. L. Molecular Beam Epitaxy and Electronic Structure of Atomically Thin Oxyselenide Films. *Adv. Mater.* **2019**, *31* (39), 1901964.

(28) Han, J. Y.; Han, X. W.; Zhang, C. Y.; Peng, S. L.; Han, C.; Zhang, X. C.; Liu, X. C.; Du, X. Y.; Gou, J.; Wang, J. Deciphering the photocurrent polarity of Bi_2O_2Se heterojunction phototransistors to enhance detection performance. *J. Mater. Chem. C* **2021**, *9* (25), 7910−7918.

(29) Luo, P.; Zhuge, F. W.; Wang, F. K.; Lian, L. Y.; Liu, K. L.; Zhang, J. B.; Zhai, T. Y. PbSe Quantum Dots Sensitized High-Mobility Bi_2O_2Se Nanosheets for High-Performance and Broadband Photodetection Beyond 2 μm. *ACS Nano* **2019**, *13* (8), 9028−9037.

(30) Hossain, M. T.; Das, M.; Ghosh, J.; Ghosh, S.; Giri, P. K. Understanding the interfacial charge transfer in the CVD grown $Bi_2O_2Se/CsPbBr_3$ nanocrystal heterostructure and its exploitation in superior photodetection: experiment vs. theory. *Nanoscale* **2021**, *13* (35), 14945−14959.

(31) Fan, C.; Dai, B. B.; Liang, H. K.; Xu, X.; Qi, Z. D.; Jiang, H. T.; Duan, H. G.; Zhang, Q. L. Epitaxial Growth of 2D Bi_2O_2Se Nanoplates/1D $CsPbBr_3$ Nanowires Mixed-Dimensional Hetero-structures with Enhanced Optoelectronic Properties. *Adv. Funct. Mater.* **2021**, *31* (16), 2010263.

(32) Rathore, E.; Kundu, K.; Maji, K.; Das, A.; Biswas, K. Mixed-Dimensional Heterostructure of $CsPbBr_3$ Nanocrystal and Bi_2O_2Se Nanosheet. *J. Phys. Chem. C* **2021**, *125* (48), 26951−26957.

(33) Yang, C. M.; Chen, T. C.; Verma, D.; Li, L. J.; Liu, B.; Chang, W. H.; Lai, C. S. Bidirectional All-Optical Synapses Based on a 2D $Bi_2O_2Se/Graphene$ Hybrid Structure for Multifunctional Optoelec-tronics. *Adv. Funct. Mater.* **2020**, *30* (30), 2001598.

(34) Liu, X.; Wang, W. H.; Yang, F.; Feng, S. P.; Hu, Z. L.; Lu, J. P.; Ni, Z. H. Bi_2O_2Se/BP van der Waals heterojunction for high performance broadband photodetector. *Sci. China Inf. Sci.* **2021**, *64* (4), 140404.

(35) Liu, S. Y.; He, D. W.; Tan, C. W.; Fu, S. H.; Han, X. X.; Huang, M. H.; Miao, Q.; Zhang, X. X.; Wang, Y. S.; Peng, H. L.; Zhao, H. Charge Transfer Properties of Heterostructures Formed by Bi_2O_2Se and Transition Metal Dichalcogenide Monolayers. *Small* **2022**, *18* (7), 2106078.

(36) Xue, X.; Ling, C.; Ji, H.; Wang, J.; Wang, C.; Lu, H.; Liu, W. Self-Powered and Broadband Bismuth Oxyselenide/p-Silicon Hetero-junction Photodetectors with Low Dark Current and Fast Response. *ACS Appl. Mater. Interfaces* **2023**, *15* (4), 5411−5419.

(37) Yang, T.; Li, X.; Wang, L. M.; Liu, Y. M.; Chen, K. J.; Yang, X.; Liao, L.; Dong, L.; Shan, C. X. Broadband photodetection of 2D $Bi_2O_2Se-MoSe_2$ heterostructure. *J. Mater. Sci.* **2019**, *54* (24), 14742−14751.

(38) Luo, P.; Wang, F. K.; Qu, J. Y.; Liu, K. L.; Hu, X. Z.; Liu, K. W.; Zhai, T. Y. Self-Driven WSe_2/Bi_2O_2Se Van der Waals Heterostructure Photodetectors with High Light On/Off Ratio and Fast Response. *Adv. Funct. Mater.* **2021**, *31* (8), 2008351.

(39) Fang, C. C.; Han, J. F.; Yu, M.; Liu, W. L.; Gao, S. M.; Huang, K. WS_2/Bi_2O_2Se van der Waals Heterostructure with Straddling Band Configuration for High Performances and Broadband Photodetector. *Advanced Materials Interfaces* **2022**, *9* (9), 2102091.

(40) Yang, S. J.; Luo, P.; Wang, F. K.; Liu, T.; Zhao, Y. H.; Ma, Y.; Li, H. Q.; Zhai, T. Y. Van der Waals Epitaxy of Bi_2Te_2Se/Bi_2O_2Se Vertical Heterojunction for High Performance Photodetector. *Small* **2022**, *18* (6), 2105211.

(41) Yu, M.; Fang, C. C.; Han, J. F.; Liu, W. L.; Gao, S. M.; Huang, K. Construction of Bi_2O_2Se/Bi_2Se_3 Van Der Waals Heterostructures for Self-Powered and Broadband Photodetectors. *ACS Appl. Mater. Interfaces* **2022**, *14* (11), 13507−13515.

(42) Wang, W. J.; Meng, Y.; Wang, W.; Zhang, Z. M.; Xie, P. S.; Lai, Z. X.; Bu, X. M.; Li, Y. Z.; Liu, C. T.; Yang, Z. B.; Yip, S.; Ho, J. C. Highly Efficient Full van der Waals 1D p-Te/2D n-Bi_2O_2Se Heterodiodes with Nanoscale Ultra-Photosensitive Channels. *Adv. Funct. Mater.* **2022**, *32* (30), 2203003.

(43) Tao, L.; Li, S. N.; Yao, B.; Xia, M. J.; Gao, W.; Yang, Y. J.; Wang, X. Z.; Huo, N. J. Raman Anisotropy and Polarization-Sensitive

Photodetection in 2D Bi_2O_2Se-WSe_2 Heterostructure. *ACS Omega* **2021**, *6* (50), 34763−34770.

(44) Chen, Y.; Tan, C.; Wang, Z.; Miao, J.; Ge, X.; Zhao, T.; Liao, K.; Ge, H.; Wang, Y.; Wang, F.; Zhou, Y.; Wang, P.; Zhou, X.; Shan, C.; Peng, H.; Hu, W. Momentum-matching and band-alignment van der Waals heterostructures for high-efficiency infrared photo-detection. *Sci. Adv.* **2022**, *8* (30), No. eabq1781.

(45) Grillo, A.; Pelella, A.; Faella, E.; Giubileo, F.; Sleziona, S.; Kharsah, O.; Schleberger, M.; Di Bartolomeo, A. Memory effects in black phosphorus field effect transistors. *2D Materials* **2022**, *9* (1), 015028.

(46) Kumar, A.; Viscardi, L.; Faella, E.; Giubileo, F.; Intonti, K.; Pelella, A.; Sleziona, S.; Kharsah, O.; Schleberger, M.; Di Bartolomeo, A. Black phosphorus unipolar transistor, memory, and photodetector. *J. Mater. Sci.* **2023**, *58* (6), 2689−2699.

(47) Sun, Y. M.; Gao, W.; Li, X. P.; Xia, C. X.; Chen, H. Y.; Zhang, L.; Luo, D. X.; Fan, W. J.; Huo, N. J.; Li, J. B. Anti-ambipolar behavior and photovoltaic effect in p-$MoTe_2$/n-InSe heterojunctions. *J. Mater. Chem. C* **2021**, *9* (32), 10372−10380.

(48) Xiong, J. X.; Sun, Y. M.; Wu, L. W.; Wang, W. Z.; Gao, W.; Huo, N. J.; Li, J. B. High Performance Self-Driven Polarization-Sensitive Photodetectors Based on GeAs/InSe Heterojunction. *Adv. Opt. Mater.* **2021**, *9* (20), 2101017.

(49) Gao, W.; Zheng, Z. Q.; Li, Y. T.; Xia, C. X.; Du, J.; Zhao, Y.; Li, J. B. Out of plane stacking of InSe-based heterostructures towards high performance electronic and optoelectronic devices using a graphene electrode. *J. Mater. Chem. C* **2018**, *6* (46), 12509−12517.

(50) Li, X. P.; Zhai, B. X.; Song, X. H.; Yan, Y.; Li, J. B.; Xia, C. X. Two-dimensional Janus-In_2STe/InSe heterostructure with direct gap and staggered band alignment. *Appl. Surf. Sci.* **2020**, *509*, 145317.

(51) Shang, H. M.; Chen, H. Y.; Dai, M. J.; Hu, Y. X.; Gao, F.; Yang, H. H.; Xu, B.; Zhang, S. C.; Tan, B. Y.; Zhang, X.; Hu, P. A. A mixed-dimensional 1D Se-2D InSe van der Waals heterojunction for high responsivity self-powered photodetectors. *Nanoscale horiz.* **2020**, *5* (3), 564−572.

(52) Hong, C. Y.; Tao, Y.; Nie, A. M.; Zhang, M. H.; Wang, N.; Li, R. P.; Huang, J. Q.; Huang, Y. Q.; Ren, X. M.; Cheng, Y. C.; Liu, X. L. Inclined Ultrathin Bi_2O_2Se Films: A Building Block for Functional van der Waals Heterostructures. *ACS Nano* **2020**, *14* (12), 16803−16812.

(53) Yan, Y.; Li, S. S.; Du, J.; Yang, H.; Wang, X. T.; Song, X. H.; Li, L. X.; Li, X. P.; Xia, C. X.; Liu, Y. F.; Li, J. B.; Wei, Z. M. Reversible Half Wave Rectifier Based on 2D InSe/GeSe Heterostructure with Near-Broken Band Alignment. *Advanced Science* **2021**, *8* (4), 1903252.

(54) Liu, H.; Zhu, X.; Sun, X.; Zhu, C.; Huang, W.; Zhang, X.; Zheng, B.; Zou, Z.; Luo, Z.; Wang, X.; Li, D.; Pan, A. Self-Powered Broad-band Photodetectors Based on Vertically Stacked WSe_2/Bi_2Te_3 p−n Heterojunctions. *ACS Nano* **2019**, *13* (11), 13573−13580.

(55) Wu, F.; Li, Q.; Wang, P.; Xia, H.; Wang, Z.; Wang, Y.; Luo, M.; Chen, L.; Chen, F. S.; Miao, J. S.; Chen, X. S.; Lu, W.; Shan, C. X.; Pan, A. L.; Wu, X.; Ren, W. C.; Jariwala, D.; Hu, W. D. High efficiency and fast van der Waals hetero-photodiodes with a unilateral depletion region. *Nat. Commun.* **2019**, *10*, 4663.

(56) Zhong, J. H.; Wu, B. A.; Madoune, Y.; Wang, Y. P.; Liu, Z. W.; Liu, Y. P. $PdSe_2$/$MoSe_2$ vertical heterojunction for self-powered photodetector with high performance. *Nano Res.* **2022**, *15* (3), 2489−2496.

(57) Gao, W.; Zheng, Z. Q.; Huang, L.; Yao, J. D.; Zhao, Y.; Xiao, Y.; Li, J. B. Self-Powered $SnS_{1-x}Se_x$ Alloy/Silicon Heterojunction Photodetectors with High Sensitivity in a Wide Spectral Range. *ACS Appl. Mater. Interfaces* **2019**, *11* (43), 40222−40231.

(58) Long, M. S.; Wang, P.; Fang, H. H.; Hu, W. D. Progress, Challenges, and Opportunities for 2D Material Based Photodetectors. *Adv. Funct. Mater.* **2019**, *29* (19), 1803807.

(59) Zankat, C. K.; Pataniya, P. M.; Patel, A.; Bhakhar, S. A.; Narayan, S.; Solanki, G. K.; Patel, K. D.; Pathak, V. M.; Sumesh, C. K.; Jha, P. K. Self-powered photodetector based on $SnSe_2$/$MoSe_2$ heterostructure. *Mater. Today Energy* **2020**, *18*, 100550.

(60) Han, L. X.; Hao, M. M. Direct combining output of fiber coupled laser diodes via fiber combiner with high efficiency and multiple input ports. *Optik* **2020**, *218*, 165268.

📖 Recommended by ACS

Type-II Bi_2O_2Se/$MoTe_2$ van der Waals Heterostructure Photodetectors with High Gate-Modulation Photovoltaic Performance

Zhiying Dan, Jingbo Li, *et al.*

MARCH 29, 2023
ACS APPLIED MATERIALS & INTERFACES   READ 🔗

Growth of Multilayer WSe_2/Bi_2O_2Se Heterostructures for Photodetection without Lithography

Jun-Cheol Park, Sanghan Lee, *et al.*

MARCH 03, 2023
CRYSTAL GROWTH & DESIGN   READ 🔗

Hierarchical Nanosheet-Based $NaBiS_2$ Flowers for High-Performance and Self-Powered Broadband Photodetectors

Ping Rong, Jinzhong Wang, *et al.*

AUGUST 11, 2022
ACS APPLIED NANO MATERIALS   READ 🔗

Size-Independent Reconfigurable Logic Gate with Bismuth Oxide Based Photoelectrochemical Device

Boheng Dong, Fuxian Wang, *et al.*

FEBRUARY 27, 2023
JOURNAL OF THE AMERICAN CHEMICAL SOCIETY   READ 🔗

Get More Suggestions >